IEEE Access
Multidisciplinary | Rapid Review | Open Access Journal

Received August 18, 2019, accepted September 10, 2019, date of publication September 16, 2019,
date of current version September 26, 2019.

Digital Object Identifier 10.1109/ACCESS.2019.2941738

An Improved Adaptive Genetic Algorithm for Optimizing Pyroshock Acceleration Synthesis

WENJUAN SUN[1,2], YINGQING HUANG[1], AND HAIBO CHEN[1]

[1]CAS Key Laboratory of Mechanical Behavior and Design of Materials, Department of Modern Mechanics, University of Science and Technology of China, Hefei 230026, China

[2]Institute of Information Engineering, Anhui Xinhua University, Hefei 230088, China

Corresponding author: Haibo Chen (hbchen@ustc.edu.cn)

This work was supported in part by the National Natural Science Foundation of China (NSFC) under Grant 11772322, in part by the Equipment Priority Research Field Foundation of China under Grant 6140246030216ZK01001, and in part by the Strategic Priority Research Program of the Chinese Academy of Sciences under Grant XDB22040502.

ABSTRACT The shock response spectrum (SRS) applied to pyroshock designs and tests for space systems does not include input acceleration time history; therefore, it cannot be used directly in structural nonlinear dynamic analysis before acceleration time history is synthesized. Existing synthesis methods typically rely on certain experimental data. In this study, a combined method for pyroshock acceleration synthesis is presented using a series of wavelets at low frequencies and damped sines at medium-high frequencies in the absence of experimental data. To improve the quality of the synthesized SRS, we develop an improved adaptive genetic algorithm (IAGA) with nonlinear adaptive adjustments of crossover and mutation probabilities. Numerical tests show that combined with the developed IAGA, the new method achieves higher accuracy and practicability in the synthesis of pyroshock acceleration compared with traditional methods. This work is expected to improve the calculation accuracy of spacecraft structure response under pyroshock loads.

INDEX TERMS Genetic algorithm, optimization, pyroshock acceleration synthesis, shock response spectrum, aerospace simulation.

I. INTRODUCTION

In the design of launch vehicles and satellites, many pyroshock devices are frequently used to achieve the separation of loads, the deployment of solar panels and other appendages, and the activation of propellant valves and other systems [1], [2]. These pyroshock devices can generate a pyroshock environment with an extremely high acceleration amplitude and a wide frequency range. The acceleration amplitude can reach as high as 10^4-10^5 g within 20 ms when the frequency range is 100 Hz to 100000 Hz [3]. In general, pyroshock slightly influences the main structure of spacecraft but may result in major functional failures of electronic and optical components; ultimately, total or partial loss of a mission may occur [4]. Electronic and optical equipment must be designed with the capability to prevent pyroshock damage. In recent years, the demand for numerical simulations to predict the responses of structures against pyroshock has been increasing [5] to reduce the cost and effort required in the initial design. Thus, accurately simulating the response of components under pyroshock loading is important in the design stage of launch vehicles and satellites.

The shock response spectrum (SRS) is an effective standard tool for engineering analysis and environmental impact quantification [6]–[8]. It describes the relationship between the maximum absolute response and natural frequency of a series of single-degree-of-freedom (SDOF) oscillators in a given base excitation. SRS can be used directly as input load to solve the linear dynamic response that meets the modal superposition criteria. However, when the equipment or secondary subsystems exhibit a nonlinear dynamical behaviour, the acceleration time history that satisfies the given SRS must be used as the input load for simulation [9], [10]. In existing aerospace structural shock design and test specification documents, only the specification requirements of SRS are given, whereas temporal information is missing. Accurately reproducing the temporal information in the inverse transform is difficult due to the lack of phase information after the temporal waveform is converted to SRS.

The associate editor coordinating the review of this manuscript and approving it for publication was Mustafa Servet Kiran.

To date, some studies have focused on solving this problem. Hale and Adhami [11] researched SRS synthesis using time-frequency analysis based on experimental data. Hemez and Doebling [12] demonstrated that the prediction of the temporal moment model associated with SRS can be used to generate time histories with the same SRS characteristics as those of the original experimental signal. Hwang and Duran [13] proposed an acceleration time waveform synthesis method using the probability density function of each major parameter of the damped sinusoid. The probability density function was obtained through the statistical analysis of considerable experimental data of spacecraft separation shock experiments. Chong *et al.* [14] presented a laser shock signal reconstruction method for simulating the separation shock waveform under point source explosion. On the basis of this study, Kim *et al.* [15] reconstructed the shock waveform of line source explosion separation. Shi *et al.* [16] used a local mean decomposition method to decompose the measured pyroshock waveform and generate a pyroshock test environment that satisfies the given SRS via cluster analysis and optimization combination.

However, all the aforementioned methods rely on a considerable amount of experimental data. Synthesizing temporal waveforms that satisfy the specified SRS without experimental signals to guide the initial design of spacecraft has become a major problem among engineers. To date, minimal research on synthesizing temporal waveforms has been conducted without sufficient experimental data. In the absence of experimental data, the simplest approach to synthesize the major characteristics of SRS is through simple shocks (e.g., half-sine, rectangular shock, or saw-toothed pulses). However, these simple shocks recreate only the most salient feature of SRS. To impose the same damage as an actual pyroshock, the summation of either damped sine terms or wavelets is becoming the most common technique for waveform synthesis [7], [8]. Ma *et al.* [17] used a genetic algorithm (GA) to optimize the waveform parameters of damped sine waves in SRS time domain synthesis. The results are within the given tolerance range, which indicates the feasibility using GA in SRS synthesis optimization. However, the substantial difference between the results and the target SRS indicates that solving similar optimization problems can still be considerably improved. Monti and Gasbarri [18] attempted to improve matching degree with the target SRS using a combined GA and sequential quadratic programming optimization method, but the results were not ideal. In their method, the modal characteristics of the analyzed structure should be obtained beforehand. Brake [19] developed a method for calculating the inverse of an arbitrary SRS using three sets of well-characterized basis functions, namely, an impulse function, a sine function/damped sine function, and a modified Morlet wavelet, in which only the SRS specified data are available. Although SRS is well matched with the target spectrum via GA optimization, Alexander [9] indicated that the ''manufactured'' waveform differs considerably from the actual pyroshock. The aforementioned analysis shows that an acceleration synthesis method that can obtain consistent results compared with a real pyroshock wave and that can improve matching accuracy between the obtained SRS and the specified SRS should be developed.

The quality of a synthesized SRS is a minimum optimization problem that is evaluated by comparing it with the target SRS. GA can be used to solve such optimization problems [17]–[19], but its optimization results easily fall into local optimal values because of its fixed crossover and mutation probabilities. In the optimization field, adaptive GA (AGA) with adaptive crossover and mutation probabilities has been developed to strengthen the global optimization capability of GA [20]–[26]. Nevertheless, existing AGAs still exhibit the shortcomings of prematurity, slow convergence, and low stability; thus, a more efficient algorithm is necessary. A key point of the current work is to propose an improved AGA (IAGA) to help the algorithm jump out of the local optimal solution and overcome the shortcoming of prematurity. The benefit of using this novel IAGA in optimizing pyrotechnic acceleration synthesis via the proposed combined synthesis method is expected to improve the calculation accuracy of structural response under pyroshock loads. The proposed IAGA is also applicable to other optimization problems.

The remainder of this paper is organized as follows. The basic acceleration synthesis methods based on damped sine and wavelet waveforms are presented in Section II. Section III describes the optimization process via GA, which is illustrated by comparing the numerical results of three examples. Section IV demonstrates the newly combined acceleration synthesis method and explains the importance of crossover and mutation probabilities by comparing the numerical results before and after parameter sensitivity analysis. Section V presents the new IAGA based on the analysis of existing AGAs. Section VI applies IAGA to the optimization of pyroshock acceleration synthesis. Section VII provides the conclusions.

II. BASIC ACCELERATION SYNTHESIS METHOD

SRS transforms time domain impact excitation into frequency domain representation, which can be defined in the form of displacement, velocity, or acceleration. Among different types of SRS, absolute acceleration SRS (AASRS) has been commonly used for shock test specifications and environment adaptability design in aerospace, electronics, and other industries [1], [8], [27]. AASRS is a calculation function based on acceleration time history that reflects mapping between acceleration shock excitation in the time domain and the maximum absolute acceleration response in the frequency domain. Acceleration time domain excitation is applied to a series of SDOF oscillators with different natural frequencies. The improved slope-invariant digital filter recursive algorithm proposed by Smallwood [28] has become a commonly used numerical algorithm and engineering standard for SRS [29], [30] because of its clear physical meaning, concise

algorithm, fast calculation speed, and high computational accuracy.

Two most commonly used techniques for waveform synthesis to satisfy a given AASRS are the summation of damped sines or wavelets because they are near actual shock acceleration waveforms [7], [8].

The basic signal is a simple exponentially damped sine wave as shown in (1) [8].

$$W_m(t) = \begin{cases} 0, & t < t_{dm} \\ A_m \exp[-\xi_m \omega_m (t - t_{dm})] & \\ \quad \sin[\sqrt{1-\xi_m^2}\,\omega_m (t - t_{dm})], & t \geq t_{dm} \end{cases} \tag{1}$$

This model is characterized by four parameters per mode: magnitude A_m, angular frequency ω_m ($\omega_m = 2\pi f_m$, f_m is the frequency), damping ξ_m, and delay time relative to zero time t_{dm}.

Acceleration can also be synthesized using a series of wavelets. An individual wavelet can be defined as (2) [8].

$$W_m(t) = \begin{cases} 0, & t < t_{dm} \\ A_m \sin[\dfrac{2\pi f_m}{N_m}(t - t_{dm})] & \\ \quad \sin[2\pi f_m (t - t_{dm})], & t_{dm} \leq t \leq t_{dm} + \dfrac{N_m}{2f_m} \\ 0, & t > t_{dm} + \dfrac{N_m}{2f_m} \end{cases} \tag{2}$$

where A_m is the wavelet acceleration amplitude, f_m is the wavelet frequency, N_m is the number of half-sines in the wavelet (an odd integer, $N_m \geq 3$), and t_{dm} is the wavelet time delay.

Total acceleration at any time t for a set of n damped sines or wavelets can be expressed as (3).

$$\ddot{Y}(t) = \sum_{m=1}^{n} W_m(t) \tag{3}$$

where m is the ordinal of the analysis frequency point, and n is the total frequency points with a resolution of at least 1/6 octave band for the natural frequency range of the AASRS test specification [1].

The time domain acceleration waveform can be obtained from Formulas (1) (or (2)) and (3). This information indicates that the total acceleration time waveform is determined by the key parameters of each waveform: A_m, ξ_m, f_m, and t_{dm} for damped sines and A_m, f_m, N_m, and t_{dm} for wavelets. Different total acceleration time waveforms can be obtained using various parameter combinations. Therefore, the selection of appropriate parameters to fulfill a given AASRS is a trial-and-error process.

III. OPTIMIZATION OF ACCELERATION SYNTHESIS VIA GA

A. OPTIMIZATION PROCESS

The AASRS value at frequency point f_m marked as SRS (f_m) of the synthetic acceleration can be obtained using the calculation method described in Section II. The value of the target AASRS at frequency point f_m is denoted as SRS_0 (f_m). A value of SRS (f_m) close to SRS_0 (f_m) indicates excellent results. A number of combinations of the key parameters are presented in the acceleration waveforms. Searching for the optimal solution via exhaustive and successive iterations is time-consuming and laborious, and a better approach is to adopt an optimization algorithm. Therefore, the problem can be transformed into an optimization problem of finding the optimal solution.

TABLE 1. Variation ranges of the decision variables.

Optimization variable	Variation range
A_m	(1/4 to 1/3)$A_0(g)$
t_{dm}	$[0.0001, t_d](s)$
ξ_m	$[0.001, 0.1]$
N_m	[5, 27] (odd number)

The objective function that should be optimized is defined as (4).

$$F = \min(\sum_{m=1}^{n} |SRS(f_m) - SRS_0(f_m)|) \tag{4}$$

where n is the number of frequency points obtained at 1/6 octave intervals within the desired frequency range. The minimum value of (4) is the target optimal solution.

GA is a search procedure based on the mechanism of natural selection and natural genetics [31]–[33]. GA is used to solve the optimization problem for acceleration synthesis. The key parameters affect a single acceleration waveform are used as decision variables. Three identical parameters are present in the two waveforms, namely, magnitude A_m, frequency f_m, and delay time t_{dm}. An SRS ($Q = 10$) performed on a shock signal has an amplitude of approximately 3 to 4 times higher than the maximum value of the acceleration time history because of the transient nature of the signal [34]. Therefore, the amplitude of the acceleration time history for a damped sine and wavelet is 1/4 to 1/3 of the amplitude of the target SRS. Thus, A_m = (1/4 to 1/3) A_0 (A_0 is the amplitude of the target SRS). Frequency f_m is related to the selected computational frequency range, and the specific value depends on the target SRS. t_{dm} is the delay time relative to zero time and typically assumes a small value from 0.0001 to t_d (waveform duration). Two different parameters are found in the two waveforms, namely, damping ξ_m in the damped sine and N_m in the wavelet. For the damped sine, $0.001 \leq \xi_m \leq 0.1$. For the wavelet, $0.001 \leq N_m \leq 0.1$. The values of the decision variables are provided in Table 1.

GA is initialized to perform optimization with the following settings:

(1) Population size is 50 to allow a large variety among subpopulations.
(2) The initial population is formed by setting the variables randomly within the value range (Table 1) for each parameter.

TABLE 2. Specification of the target SRS.

Near field		Middle field		Far field	
Frequency (Hz)	Amplitude (g)	Frequency (Hz)	Amplitude (g)	Frequency (Hz)	Amplitude (g)
100	300	100	60	100	50
1000	3000	2000	3000	1000	1000
3000	10000	10000	3000	10000	1000
10000	10000				

(3) The maximum generation size is set to 500.
(4) The selection operation is tournament selection, and the tournament size is 4.
(5) The crossover probability P_c and mutation probability P_m are selected with the empirical values of 0.85 and 0.01 [35], respectively.
(6) The stopping criteria for GA are as follows: the maximum number of generations is reached or the cumulative change in the fitness value maintains a value of at least 1.0×10^{-10}.

B. CASE STUDY

The pyroshock environment can be divided into near, middle, and far fields in accordance with the magnitude of shock response and the spectrum components following the source type and size or strength and the distance from the pyroshock source. The pyroshock environment is mostly distributed within the frequency range of 100 Hz to 10000 Hz, which is generally selected to analyze SRS response in engineering. Three typical AASRS from the far, middle, and near fields are selected as the target SRS and listed in Table 2.

The total duration of the pyroshock acceleration that should be synthesized is determined using (5) [36].

$$t = \frac{1.5}{f_{min}} = \frac{1.5}{100} = 0.015 \tag{5}$$

where f_{min} is the lowest frequency in the target SRS.

In using the three standard spectra in Table 2 as target SRS, 41 frequency points are selected in the frequency band of 100 Hz to 10000 Hz with 1/6 octave intervals (the f_m values are 100, 112, 126, 141, 160, 178, 200, 224, 252, 283, 317, 356, 400, 449, 504, 566, 635, 713, 800, 898, 1008, 1131, 1270, 1425, 1600, 1800, 2016, 2263, 2540, 2851, 3200, 3529, 4032, 4525, 5080, 5702, 6400, 7184, 8063, 9051, and 10000). That is, $n = 41$ in (3). The tolerance that is most commonly used in current aerospace applications is assumed to be −3 dB/+6 dB across the full spectrum [8].

The acceleration synthesis of the three target SRS in Table 2 is optimized using the aforementioned optimization method. To minimize evaluation noise from the possible contingency of randomness and nondeterminism, each program is executed 20 times with the same parameter settings. The number of 20 runs is selected as a compromise between the number of replicates for statistically significant results and the computation time required to repeat GA runs [37]. The comparison results of the two waveforms of damped sine and wavelet are presented in Fig. 1.

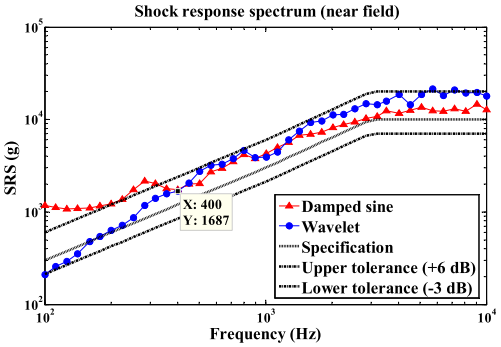

(a) Near field

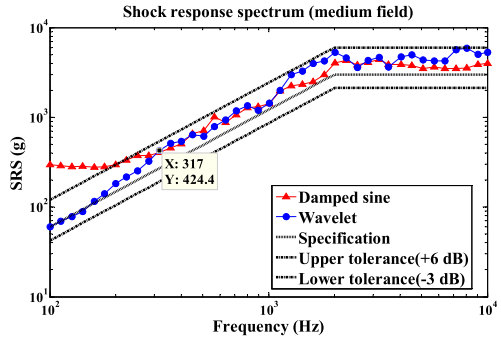

(b) Medium field

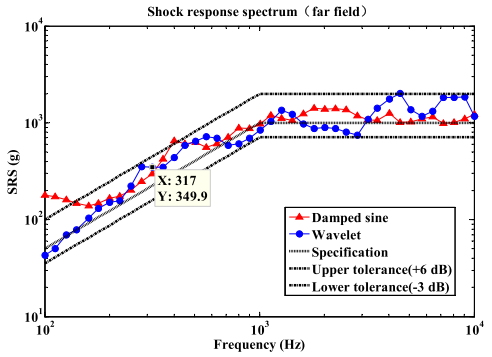

(c) Far field

FIGURE 1. Comparison results of damped sine and wavelet.

As indicated in Fig. 1, the synthesized SRS from the damped sine acceleration waveform is closer to the SRS specification than the wavelet at medium to high frequencies (above 317 Hz). By contrast, the wavelet acceleration waveform moves the SRS closer to the SRS specification than the damped sine at low frequencies. The results clearly indicate that the wavelet is appropriate for low-frequency pyroshocks, whereas the damped sine is suitable for medium-high frequency pyroshocks.

IV. NEW COMBINED APPROACH FOR SYNTHESIZING PYROSHOCK ACCELERATION

A. NEW PROCESSING METHOD

In this section, a new combined synthesis method for the pyroshock acceleration time domain waveform is proposed

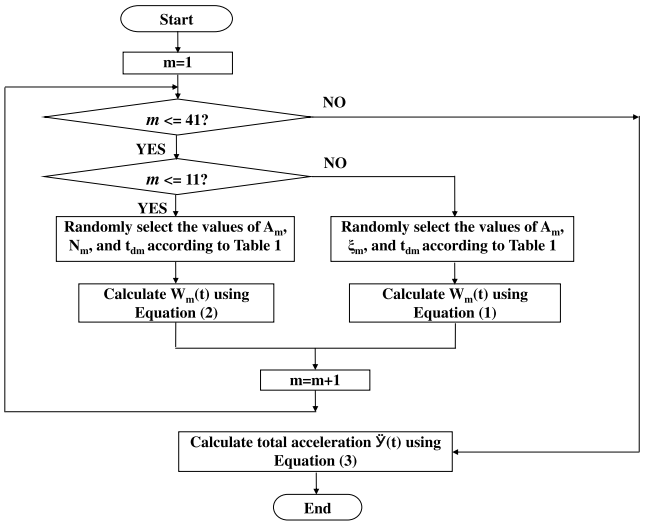

FIGURE 2. Flowchart of the new combined approach for synthesizing pyroshock acceleration signals.

with the wavelet in the low frequency range and the damped sine in the medium-high frequency range. In the frequency range of 100 Hz to 10000 Hz with 1/6 octave interval, the frequency points below 400 Hz are 100, 112, 126, 141, 160, 178, 200, 224, 252, 283, 317, 356, and 400. Considering the calculation results of the three comparative examples in Section III, the 11 frequency points of 100, 112, 126, 141, 160, 178, 200, 224, 252, 283, and 317 Hz adopt wavelet synthesis, whereas the 30 other frequency points between 356-10000 Hz use the damped sine waveform. The specific operations are as follows. In (3), when synthesizing acceleration, $m = 1 - 11$ using (2); $m = 12 - 41$ using (1). The flowchart of the new combined approach for synthesizing pyroshock acceleration signals is presented in Fig. 2.

B. OPTIMAL COMPUTATION BY GA

The proposed new method (marked as wavelet & damped sine) is used to recalculate the SRS of the three specifications in Table 2. The comparison results obtained via GA are shown in Fig. 3.

The average value, best optimal value, and standard deviation of the final optimization objective function (4) calculated 20 times in the three examples are listed in Table 3.

As shown in Fig. 3 and Table 3, the results of the proposed new hybrid method are considerably closer to the target pyrotechnic SRS than those of the traditional methods of wavelet or damped sine alone. Moreover, the values of the objective function (4) of the new method are the smallest among the three methods. Nevertheless, the matching degree for the target SRS is not very good, and some frequency points exceed the tolerance range of −3 dB/+6 dB. This phenomenon may be attributed to the use of empirical values of the crossover probability P_c and mutation probability P_m of GA, and the two probabilities remain constant throughout the optimization process. However, whether the values of P_c and

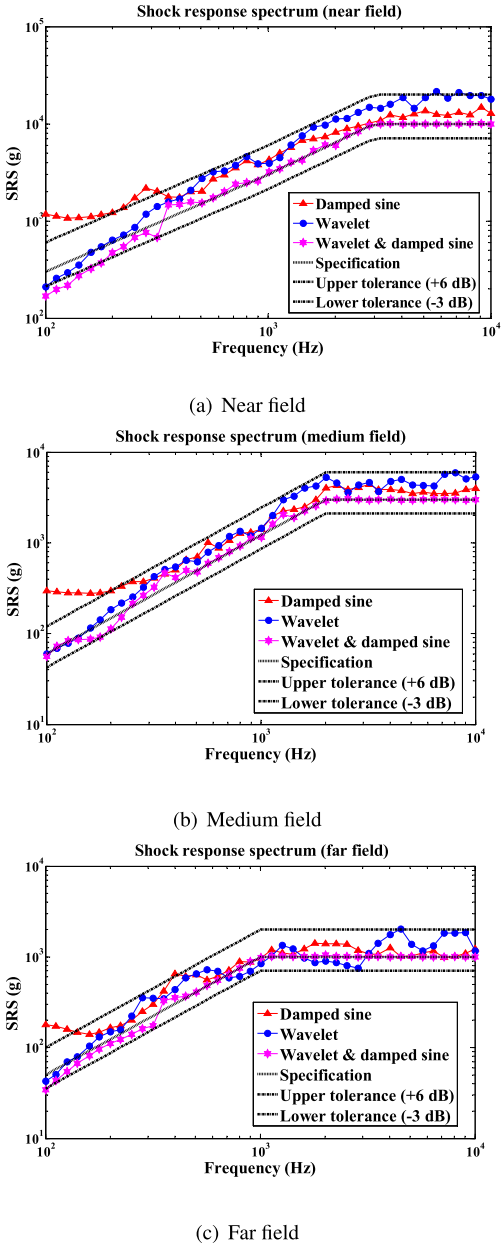

FIGURE 3. Comparison results among damped sine, wavelet, and the proposed new method.

P_m exert considerable influences on the final optimization results requires further investigation.

C. SENSITIVITY ANALYSIS OF P_c AND P_m

In the optimization process of GA, a large value of P_c indicates the fast generation of new individuals. However, an excessively large P_c may destroy the genetic model. By contrast, a small value of P_c implies a slow search process; an excessively small P_c will cause evolution to stagnate. The suitable value of P_c is between 0.3 and 0.9 [20]. The mutation probability P_m controls the speed at which new genes are introduced into the population. P_m should be appropriate to ensure the diversity of individuals. In the current application

TABLE 3. Comparison results among wavelet, damped sine, and the proposed method (SD: Standard deviation, W&D: Wavelet & damped sine).

Method	Near field			Middle field			Far field		
	Average	Best	SD	Average	Best	SD	Average	Best	SD
Wavelet	1.461e03	634.166	500.304	444.838	254.013	119.044	183.072	93.742	53.196
Damped sine	162.735	138.675	27.145	97.852	61.233	41.529	36.051	23.599	8.513
W&D	**137.549**	**90.955**	**26.745**	**53.369**	**30.342**	**12.352**	**29.217**	**17.775**	**5.261**

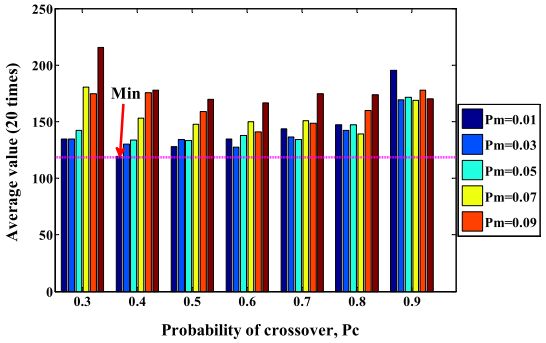

FIGURE 4. Parameter sensitivity analysis results.

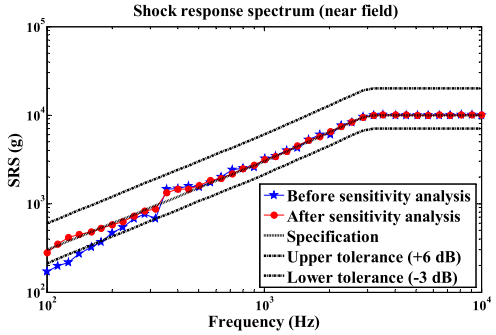

FIGURE 5. Comparison results between empirical and optimization parameters for near-field SRS.

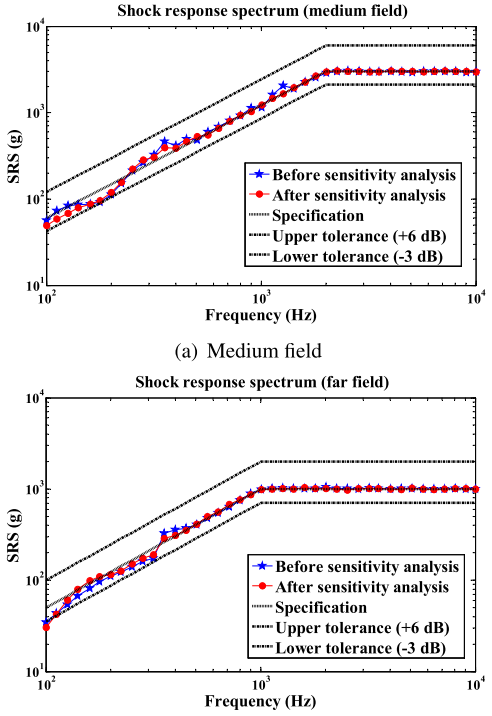

FIGURE 6. Comparison results between empirical and optimization parameters for medium and far fields.

of GA to optimization problems, a fixed small value of P_m between 0.01 and 0.1 is adopted. The acceleration synthesis optimization problem of near-field SRS is selected, and the parameter sensitivity analysis of the values of P_c and P_m is conducted. P_c is set between 0.3 and 0.9 with an interval of 0.1, whereas P_m is set between 0.01 and 0.09 with an interval of 0.02. The average result of 20 calculations is presented in Fig. 4.

As shown in the figure, $P_c = 0.4$ and $P_m = 0.01$ are the optimal parameters of GA for the near-field target SRS. The near-field acceleration synthesis problem is reoptimized, and the comparison results with Section 4.2 using empirical $P_c = 0.85$ and $P_m = 0.01$ are presented in Fig. 5.

As shown in Fig. 5, the SRS obtained after parameter sensitivity analysis is closer to the target SRS than the empirical parameters. Furthermore, the value at each frequency point is completely consistent with the target specification SRS. At this point, we conclude that the values of P_c and P_m considerably affect the optimization results.

To better supporting this conclusion, we use the parameter set ($P_c = 0.4, P_m = 0.01$) to optimize the two other examples of the middle and far fields. The comparison results of the SRS curves are shown in Fig. 6.

The figure indicates that the optimized combination of parameters does not improve the results of the middle and far fields as those of the near field. The results calculated using the empirical parameters are nearly the same as those calculated using the optimization parameters. Some data are far from the specification at many points in the low frequency range, whereas other data exceed the tolerance range of -3 dB/$+6$ dB. This situation occurs because the combination ($P_c = 0.4, P_m = 0.01$) obtained by the parameter sensitivity analysis is based on the near-field target SRS. However, when this set of parameters is applied to the middle and far fields of different problems, their advantages disappear.

The aforementioned comparative analysis results show that the values of P_c and P_m in GA exert an important influence on the optimization results. For different problems, the optimal parameter combination also varies even if slight

differences occur. No uniform parameter exists for all problems. Thus, the most suitable GA parameters should be identified for each problem.

V. IAGA

The performance of GA depends considerably on P_c and P_m, which largely determine whether GA can efficiently find an optimal or near-optimal solution [38]. A poorly selected P_c and P_m may lead GA to converge prematurely to sub-optimal solutions or direct it to search too widely for the fitness function without fully using current knowledge to find improved solutions. However, identifying values for P_c and P_m to produce near-optimal solutions remains a difficult task. Values are generally found using a trial-and-error approach, which can be extremely time-consuming. Given that GA is easily trapped in a local optimum, AGA is used, in which P_c and P_m can be adjusted adaptively such that the fitness value changes to help the algorithm converge to the globally optimal solution [20]–[26], [39].

A. AGA

The adaptive ability of GA should be reflected in the capability of individuals in a population to automatically find the characteristics and laws of the environment depending on the changes in the surrounding environment. The most obvious environmental feature is the fitness of an individual, whereas the most evident evolution rule is the relationship between individual and average fitness values and the minimum and maximum fitness values in a population. In the evolution process, an organism does not remember the generation to which it has evolved, but whether it has improved its ability to adapt to the environment should be a concern. If an improvement occurs, then a good pattern is found, and this pattern should be preserved as much as possible in the algorithm design. Otherwise, the pattern is likely to be eliminated by nature.

The major difference between traditional GA and AGA is the selection of P_c and P_m. In conventional GA, the two probabilities are randomly determined or based on a preset reference. By contrast, AGA relies on the fitness function to select optimal values. Several versions of AGA are found in the literature. Since the first introduction of AGA by Srinivas and Patnaik [20] in 1994, many researchers have proposed improved methods for AGA [21]–[26]. In order to describe the improved AGA proposed in our paper conveniently, the improved methods in references [21]–[26] are still labeled as AGA. In accordance with the adjustment methods for P_c and P_m, AGA can be classified into two categories: dynamic linear [21]–[23] and nonlinear [24]–[26] adjustments.

1) LINEAR ADJUSTMENT OF AGA

In this AGA, the P_c and P_m of an individual are linearly adjusted between the average and maximum or minimum fitness values on the basis of the fitness of the individual, and the minimum P_c and P_m are not zero. This type of AGA can be further divided into the following two types depending on whether the probabilities are adjustable at both branches of the average fitness value, i.e., one branch is fixed, whereas the other branch is adjusted linearly (using the average fitness value as the demarcation point) [21], [22]. Both branches are linearly adjusted [23].

(1) One branch is fixed, whereas the other is adjusted linearly (labeled as AGA-1).

(2) Both branches are linearly adjusted (labeled as AGA-2).

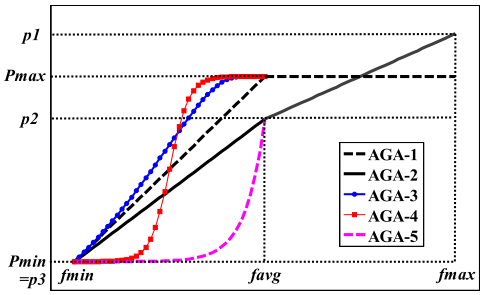

FIGURE 7. Adaptive *P* for the minimum problem.

2) NONLINEAR ADJUSTMENT OF AGA

AGA-1 and AGA-2 enable adaptive and linear adjustment of P_c and P_m. Although AGA-2 can escape from the local optimum with a higher probability than AGA-1, it does not solve the problems of local optimum and premature convergence, as reported in [24]–[26]. In the current study, the nonlinear adjustment strategy is used to avoid disadvantages, such as premature convergence, low stability, and slow convergent speed. Nonlinearly adjusted AGAs can be classified into two types depending on whether the probabilities are adjusted at both branches of the average fitness value: (1) one branch is fixed and the other is adjusted nonlinearly (using the average fitness value as the demarcation point) [24], [25] and (2) one branch is adjusted linearly, and the other is adjusted nonlinearly [26].

(1) One branch is fixed, whereas the other is adjusted nonlinearly

According to the difference nonlinear adjustment strategies, this type can be divided into two types: one is an exponential function [24], labeled as AGA-3, the other is a sigmoid function ($A = 9.903438$) [25], labeled as AGA-4.

(2) One branch is liner and the other is nonlinear (labeled as AGA-5) [26]

To improve the comparison and analysis of different AGAs, their probability adjustment curves are plotted in Fig. 7. For a convenient description, the adjustment curves for P_c and P_m are expressed in a unified manner as P because the shape of their curves is the same. In Fig. 7, f_{min}, f_{max} and f_{avg} represent the minimum, maximum and average fitness values, respectively; $P_1 > P_{max} > P_2 > P_3 \in (0, 1)$, $P_{min} = P_3$. This figure shows that the curve of P in AGA-1, AGA-2, and AGA-5 become steep when f_{avg} and f_{min} are near each other. Thus, the probabilities of these individuals considerably vary from one another even if a slight difference occurs with their individual fitness values. Thus, most

individuals only have a low P, thereby causing evolution to stagnate. To avoid the aforementioned situation, the adaptive adjustment curve of P should be first changed slowly at and near f_{avg} to considerably improve the P value of individuals with fitness close to f_{avg}. Second, the adaptive adjustment curve at f_{min} should be smoothed to ensure that better individuals in the current population will still have large enough crossover and mutation probabilities. Although the adaptive adjustment curve in AGA-3 is smooth near f_{avg}, it retains a large probability value near f_{min}, which is not conducive to retaining superior individuals in the later stage of evolution. In AGA-4, however, the adaptive curve of P varies slowly in the f_{avg} of the population, and the crossover and mutation rates of individuals close to f_{avg} are substantially improved. Simultaneously, the pattern of individuals near f_{min} is preserved as much as possible, and their probabilities are lower but higher than 0. This explains why the algorithm strives to jump out of local convergence.

B. NEW IAGA

A new IAGA based on the aforementioned comparative analysis is presented in this section.

The global optimization performance of previous AGAs can be further improved through the following three aspects. First, we smooth the adaptive adjustment curve near f_{avg} and enable the individuals close to f_{avg} to have considerably improved probability values. Second, we reduce the probability value of the individuals near f_{min} to preserve excellent individual patterns. Third, we ensure that the individuals with less than the ideal value (from f_{max} to f_{avg} for minimal optimization) maintain high crossover and mutation rates. Therefore, the values of P_c and P_m are tuned adaptively and nonlinearly at both branches via the following sigmoid function:

$$P = \begin{cases} P_3 + \dfrac{P_2 - P_3}{1 + \exp\left(A\dfrac{2(f_{avg} - f)}{f_{avg} - f_{min}} - 1\right)}, \\ \quad f_{min} < f \le f_{avg} \\ P_2 + \dfrac{P_1 - P_2}{1 + \exp\left(A\dfrac{f_{avg} + f_{max}}{2} - f \right)}, \\ \quad f_{avg} < f < \dfrac{f_{avg} + f_{max}}{2} \\ P_2 + \dfrac{P_1 - P_2}{1 + \exp\left(A(1 - \dfrac{2(f - f_{avg})}{f_{max} - f_{avg}})\right)}, \\ \quad \dfrac{f_{avg} + f_{max}}{2} < f \le f_{max} \end{cases} \tag{6}$$

where, $A = 9.903438$.

The adjustment curve of probability is presented in Fig. 8. This figure shows that the new IAGA proposed in this work causes the crossover and mutation curves to vary nonlinearly via nonlinear adjustments, which smoothes the adaptive curve at any point. The new IAGA will pull away majority of the individuals around the average fitness when the individuals are similar, which can drive the progress of evolution. This phenomenon is important in eliminating local convergence and preventing the algorithm from stalling. The optimization flowchart of the new IAGA is presented in Fig. 9.

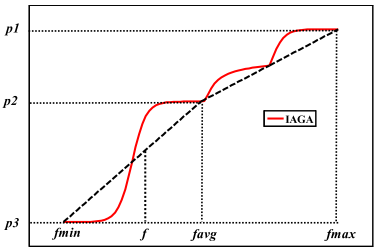

FIGURE 8. Adaptive P of the new IAGA for the minimum optimization problem.

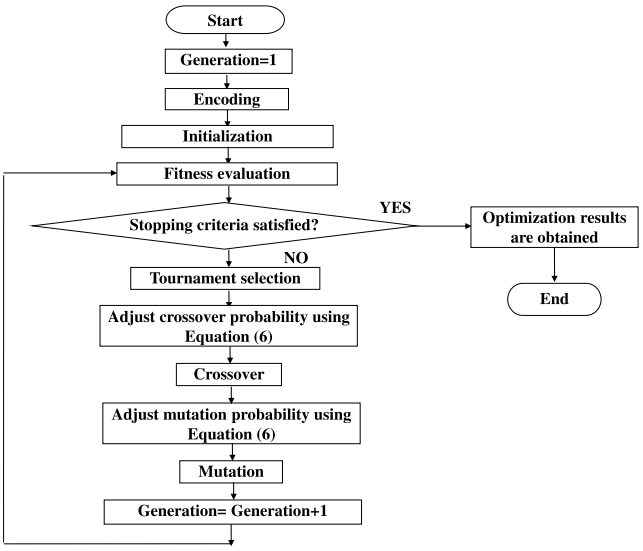

FIGURE 9. Flowchart of the new IAGA.

VI. APPLICATION OF THE NEW IAGA TO THE OPTIMIZATION OF PYROSHOCK ACCELERATION SYNTHESIS

A. OPTIMIZATION RESULTS

The new IAGA is applied to recalculate the three pyroshock acceleration synthesis examples of near-, middle- and far-field target SRS in Table 2 using the proposed synthesis method. To increase the clarity of the analysis results, the five AGAs and two other classic optimization algorithms, particle swarm optimization (PSO) and simulated annealing (SA) are selected for comparison. GA and AGA have the same parameters except for P_c and P_m. All the parameters are listed in Table 4. The evolutionary number of the five AGAs is 500 generations, and the maximum iterations of PSO and SA is 500, therefore, these nine methods are labeled as GA(500), AGA-1(500),

TABLE 4. Parameters of GA and AGA.

Parameters	Values	Parameters	Values
Population (P)	50	P_{cmax} for AGA-1, AGA-3, and AGA-4	0.75
Maximum generation (G)	500	P_{cmin} for AGA-1, AGA-3, and AGA-4	0.3
P_c for GA	0.85	P_{m1} for AGA-2, AGA-5, and IAGA	0.1
P_m for GA	0.01	P_{m2} for AGA-2, AGA-5, and IAGA	0.05
P_{c1} for AGA-2, AGA-5, and IAGA	0.9	P_{m3} for AGA-2, AGA-5, and IAGA	0.01
P_{c2} for AGA-2, AGA-5, and IAGA	0.6	P_{mmax} for AGA-1, AGA-3, and AGA-4	0.075
P_{c3} for AGA-2, AGA-5, and IAGA	0.3	P_{mmin} for AGA-1, AGA-3, and AGA-4	0.01

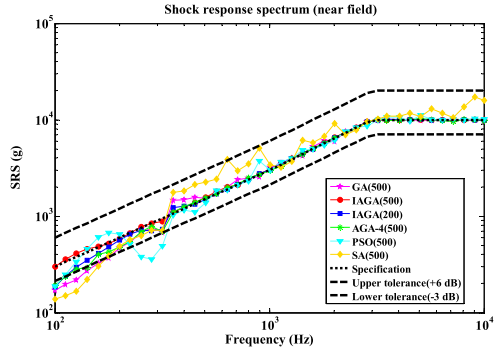

(a) Near field

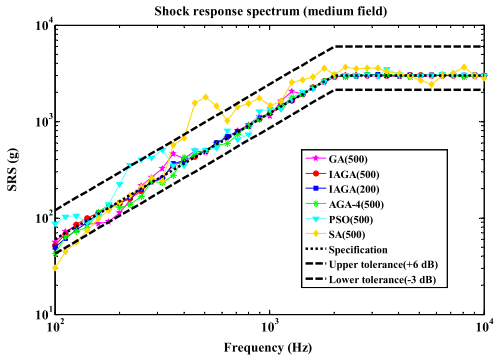

(b) Medium field

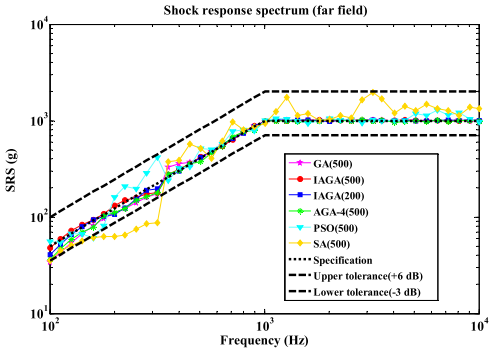

(c) Far field

FIGURE 10. Comparison results among GA, IAGA, AGA-4, PSO, and SA.

AGA-2(500), AGA-3(500), AGA-4(500), AGA-5(500), IAGA(500), PSO(500) and SA(500), respectively. Furthermore, the 200 evolutionary number of the new IAGA was added as a comparison to show the superiority of the new IAGA in terms of convergence speed, which labeled as IAGA(200). All the aforementioned results are provided in Table 5. The results in Table 5 show that the optimized values obtained by the new IAGA(500) are the smallest among the nine algorithms, followed by AGA-4(500), thereby demonstrating the advantage of the new IAGA in solving the pyroshock acceleration synthesis optimization problem. The optimization results of IAGA(200) and AGA-4(500) are equivalent; thus, the IAGA proposed in this study can improve convergence speed toward the global optimal solution. A slight difference is observed in the optimization results among various random initializations with IAGA, which can be measured by the standard deviation of 20 calculations compared in Table 5. Table 5 shows that the standard deviation of IAGA(500) in 20 calculations is the smallest, thereby indicating the stability of the algorithm and the consistency of optimization convergence. The numerical results demonstrate that the adaptively and nonlinearly tuned probabilities of P_c and P_m enable IAGA to simultaneously avoid the problems of premature, slow convergence and low stability. Furthermore, Table 5 indicates that the calculation time of IAGA(500) is slightly longer than that of AGA-4(500) and GA(500), and the increase time of the middle field is the longest, although it is only a 5.6% increase from that of GA(500). Considering the improvement and enhancement of IAGA to the optimization results, the increase in calculation time is acceptable.

To increase the clarity of the analysis results, AGA-4, which achieves the best optimization performance among the five AGAs, the conventional GA, PSO and SA are selected for graphical comparison analysis. The comparison results are provided in Fig. 10. This figure indicates that the results of IAGA(500) are considerably improved compared with those of AGA-4(500) and GA(500), and are far better than those of PSO(500) and SA(500). The obtained values of all the frequency points of IAGA(500) are within the tolerance range of -3 dB/$+6$ dB, and the matching degree with the target specification SRS is substantially better than that of AGA-4(500) and GA(500). The optimization results of IAGA(200) are better than those of GA(500), thereby demonstrating that the new IAGA exhibits the advantage of fast convergence speed. When this method is used, we can easily find the global optimal solution for solving the synthesis problem of pyroshock acceleration.

TABLE 5. Comparison results among GA, IAGA, AGAs, PSO, and SA.

Method	Near field				Middle field				Far field			
	Average	Best	SD	Time(s)	Average	Best	SD	Time(s)	Average	Best	SD	Time(s)
GA(500)	137.5490	90.9548	26.7499	297.7	53.3685	30.3419	12.3518	299.0	29.2165	17.7754	5.2607	299.7
AGA-1(500)	115.8557	85.3151	20.4581	351.6	42.6669	28.7353	8.4849	356.6	20.9901	16.9939	4.4202	366.8
AGA-2(500)	113.8151	79.6937	23.7920	347.1	35.8437	25.4056	8.9053	370.3	20.9084	16.8909	3.9467	291.3
AGA-3(500)	107.0615	76.4189	24.2404	361.8	35.6853	29.9937	8.9214	359.0	20.3375	16.065	4.165	362.5
AGA-4(500)	105.847	75.4775	17.4718	298.1	35.5530	24.264	8.3053	306.0	20.2598	15.8909	3.5668	291.3
AGA-5(500)	110.9206	92.7348	18.8243	362.0	39.7734	34.8098	8.3789	357.3	20.7755	16.6881	4.7641	354.0
IAGA(500)	**98.6308**	**69.6588**	**15.7170**	304.1	**35.2208**	**24.0709**	**7.3702**	315.8	**20.0347**	**13.0493**	**3.5571**	304.5
IAGA(200)	116.5842	85.9044	18.6452	115.7	46.3234	25.3233	7.7105	115.6	28.1184	14.2614	4.8053	112.6
PSO(500)	273.979	174.1868	69.5891	131.5	95.6448	50.6845	34.2547	111.0	46.1634	32.6482	11.446	132.86
SA(500)	1191.1	746.4516	239.697	97.53	388.462	192.717	114.164	96.26	215.024	145.341	42.099	117.31

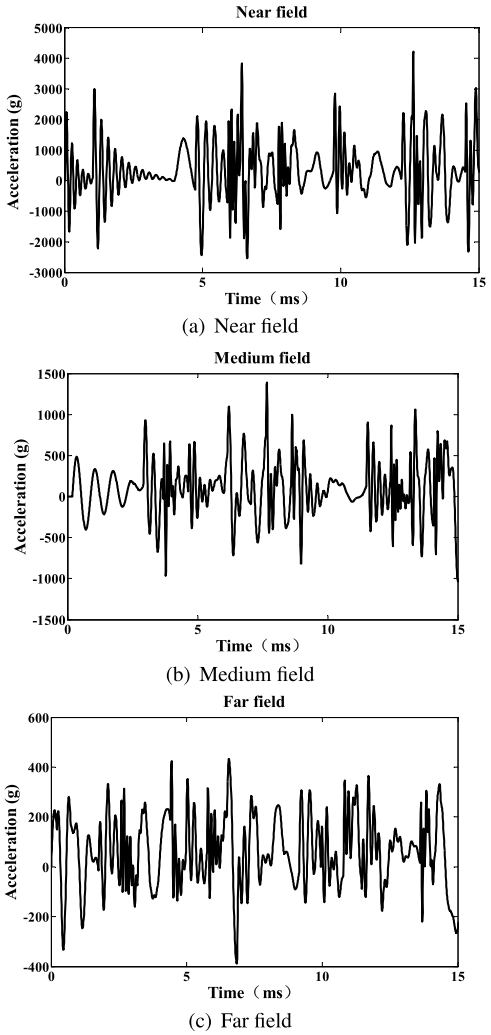

(a) Near field

(b) Medium field

(c) Far field

FIGURE 11. Acceleration time history curve.

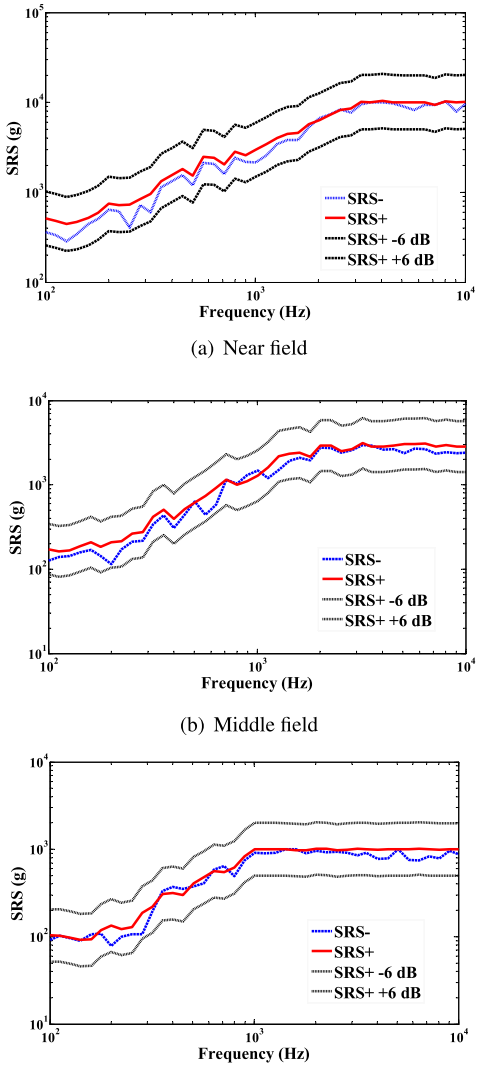

(a) Near field

(b) Middle field

(c) Far field

FIGURE 12. Comparison results of SRS+ and SRS−.

B. RATIONALITY VERIFICATION OF ACCELERATION INFORMATION

The SRS obtained via IAGA and the target SRS match each other well, but whether the synthesized acceleration information is reasonable and effective still requires verification. The relevant standard document for pyroshock design and verification [8] stipulates that the general method for judging the validity of the acceleration that characterizes pyroshock is

the consistency between positive SRS (SRS+) and negative SRS (SRS−). If the difference between SRS+ and SRS− does not exceed +/ − 6 dB at all the frequency points in a given frequency range, then the acceleration waveform is considered effective and reliable.

The acceleration time history curves obtained using IAGA are shown in Fig. 11. The curves are relatively close to the time domain waveform of pyroshock.

The SRS that corresponds to the three aforementioned accelerations is calculated using the improved slope-invariant digital filter recursive algorithm [28], and the obtained SRS+ and SRS− are presented in Fig. 12.

The results in Fig. 12 show that the acceleration obtained by the presented IAGA exhibits a difference between SRS+ and SRS− within +/ − 6 dB at all the frequency points in the given frequency band. This result demonstrates the validity and reliability of the acceleration waveform optimized by IAGA, which can be used as pyroshock load to analyze and calculate the structural response.

VII. CONCLUSION

A combined method that uses a series of wavelets at low frequencies and damped sines at medium-high frequencies is proposed for the synthesis of pyroshock acceleration in the absence of experimental data. The quality assessment of a synthesized SRS is a minimum optimization problem, which is addressed using the IAGA proposed in this work. The new IAGA is composed of crossover and mutation probabilities of adaptive and nonlinear adjustments, which make the IAGA more stable and can more easily to find the global optimal solution with fewer evolutionary generations. Although the new IAGA takes a slightly longer time than conventional GAs under the same evolutionary generation, the optimization results are considerably improved. In the comparison analysis, we demonstrate that combined with the developed IAGA, the new acceleration synthesis method can remarkably improve numerical accuracy, and the results are substantially closer to the target SRS than those of traditional methods. The obtained acceleration waveforms are close to the actual pyroshock waves and are verified by comparing the difference between SRS+ and SRS−. The synthesized acceleration waveform may be used as a base-driven input transient to a finite element model to simulate modal transient responses. Thus, the waveform is helpful in solving the problem of difficulty in predicting a pyroshock environment. This study is important for guiding anti-pyroshock design in space systems.

REFERENCES

[1] *Pyroshock Test Criteria, NASA Technical Standard. National Aeronautics and Space Administration*, NASA Technical Standard. National Aeronautics and Space Administration Stdandard, NASA-STD-7003A, Rev. NASA-STD-7003, 2011.
[2] J. Lee, J.-H. Han, Y. Lee, and H. Lee, "Separation characteristics study of ridge-cut explosive bolts," *Aerosp. Sci. Technol.*, vol. 39, pp. 153–168, Dec. 2014.
[3] J.-R. Lee, C. C. Chia, and C.-W. Kong, "Review of pyroshock wave measurement and simulation for space systems," *Measurement*, vol. 45, no. 4, pp. 631–642, 2012.
[4] A. Lacher, N. Jüngel, U. von Wagner, and A. Bäger, "Analytical calculation of in-plane response of plates with concentrated masses to impact and application to pyroshock simulation," *J. Sound Vib.*, vol. 331, no. 14, pp. 3358–3370, Jul. 2012.
[5] A. García-Pérez, F. Sorribes-Palmer, G. Alonso, and A. Ravanbakhsh, "Overview and application of FEM methods for shock analysis in space instruments," *Aerosp. Sci. Technol.*, vol. 80, pp. 572–586, Sep. 2018.
[6] M. Caresta, R. S. Langley, and J. Woodhouse, "Transient response of structures with uncertain properties to nonlinear shock loading," *J. Sound Vib.*, vol. 332, no. 22, pp. 5821–5836, 2013.
[7] *Dynamic Environmental Criteria NASA Technical Handbook*, NASA Stdandard, NASA-HDBK-7005, 2001.
[8] *Space Engineering-Mechanical Shock Design and Verification Handbook*, European Space Agency Standard, ECSS-E-HB-32-25A, 2015.
[9] J. Alexander, "A new method to synthesize a shock response spectrum compatible base acceleration to improve multi-degree of freedom system response," Ph.D. dissertation, Univ. Minnesota, Minneapolis, MN, USA, 2015.
[10] J. Lee, D.-H. Hwang, and J.-H. Han, "Study on pyroshock propagation through plates with joints and washers," *Aerosp. Sci. Technol.*, vol. 79, pp. 441–458, Aug. 2018.
[11] M. T. Hale and R. Adhami, "Time-frequency analysis of shock data with application to shock response spectrum waveform synthesis," in *Proc. Southeastcon*, Apr. 1991, pp. 213–217.
[12] F. M. Hemez and S. W. Doebling, "From shock response spectrum to temporal moments and vice-versa," in *Proc. 21st SEM Int. Modal Anal. Conf.*, 2002, pp. 1–9.
[13] J. H.-J. Hwang and A. Duran, "Stochastic shock response spectrum decomposition method based on probabilistic definitions of temporal peak acceleration, spectral energy, and phase lag distributions of mechanical impact pyrotechnic shock test data," *Mech. Syst. Signal Process.*, vols. 76–77, pp. 424–440, Aug. 2016.
[14] S. Y. Chong, J. R. Lee, and C. W. Kong, "Shock response spectra reconstruction of pointwise explosive-induced Pyroshock based on signal processing of laser shocks," *Shock Vib.*, vol. 2014, no. 1, Apr. 2014, Art. no. 695836.
[15] Y.-W. Kim, J.-K. Jang, and J.-R. Lee, "Pyroshock acceleration field reconstruction in temporal and spectral domains based on laser shock scanning and iterative decomposition and synthesis considering stop band effects," *Shock Vib.*, vol. 2017, Oct. 2017, Art. no. 8351791.
[16] P. Shi, W. Qiu, Z. Wang, R. Wu, K. Chen, and X. Wang, "A new method for time domain waveform synthesis of shock response spectrum based on local mean decomposition," (in Chinese), *Spacecraft Environ. Eng.*, vol. 35, no. 2, pp. 135–140, Apr. 2018.
[17] D. Ma, F. Zhuang, and Z. Xu, "Time-domain synthesis method for shock response spectrum based on genetic algorithm," (in Chinese), *Struct. Environ. Eng.*, vol. 42, no. 5, pp. 49–53, Oct. 2015.
[18] R. Monti and P. Gasbarri, "Dynamic load synthesis for shock numerical simulation in space structure design," *Acta Astronautica*, vol. 137, pp. 222–231, Aug. 2017.
[19] M. R. Brake, "An inverse shock response spectrum," *Mech. Syst. Signal Process.*, vol. 25, no. 7, pp. 2654–2672, 2011.
[20] M. Srinivas and L. M. Patnaik, "Adaptive probabilities of crossover and mutation in genetic algorithms," *IEEE Trans. Syst., Man, Cybern.*, vol. 24, no. 4, pp. 656–667, Apr. 1994.
[21] W.-T. Sung and C.-L. Hsiao, "IHPG algorithm for efficient information fusion in multi-sensor network via smoothing parameter optimization," *Informatica*, vol. 24, no. 2, pp. 291–313, 2013.
[22] J. Song, C. Hou, G. Xue, and M. Ma, "Study of constellation design of pseudolites based on improved adaptive genetic algorithm," *J. Commun.*, vol. 11, no. 9, pp. 879–885, 2016.
[23] M. Yan, H. Hu, Y. Otake, A. Taketani, Y. Wakabayashi, S. Yanagimachi, S. Wang, Z. Pan, and G. Hu, "Improved adaptive genetic algorithm with sparsity constraint applied to thermal neutron CT reconstruction of two-phase flow," *Meas. Sci. Technol.*, vol. 29, no. 5, 2018, Art. no. 055404.
[24] Z. Dong and M. Yang, "Optimal design of a double-vibrator ultrasonic motor using combination method of finite element method, sensitivity analysis and adaptive genetic algorithm," *Sens. Actuators A, Phys.*, vol. 266, pp. 1–8, Oct. 2017.
[25] B. Yan, C. Yan, F. Long, and X.-C. Tan, "Multi-objective optimization of electronic product goods location assignment in stereoscopic warehouse based on adaptive genetic algorithm," *J. Intell. Manuf.*, vol. 29, no. 6, pp. 1273–1285, 2018.

[26] L. Wang, "Research on emergency management capability evaluation of hazardous chemical supply chain," *Chem. Eng. Trans.*, vol. 62, pp. 1369–1374, Dec. 2017.
[27] B. W. Li and Q. M. Li, "Damage boundary of structural components under shock environment," *Int. J. Impact Eng.*, vol. 118, pp. 67–77, Aug. 2018.
[28] D. O. Smallwood, "An improved recursive formula for calculating shock response spectra," *Shock Vib. Bull.*, vol. 51, no. 2, pp. 211–217, 1981.
[29] *Mechanical Vibration and Shock-signal Processing, Part4 Shock Response Spectrum Analysis*, ISO Standard, ISO/WD-18431-4, Feb. 2007.
[30] H. Zhao, W. Liu, J. Ding, Y. Sun, X. Li, and Y. Liu, "Numerical study on separation shock characteristics of pyrotechnic separation nuts," *Acta Astronautica*, vol. 151, pp. 893–903, Oct. 2018.
[31] L. Cruz-Piris, M. A. Lopez-Carmona, and I. Marsa-Maestre, "Automated optimization of intersections using a genetic algorithm," *IEEE Access*, vol. 7, pp. 15452–15468, 2019.
[32] P. Seda, M. Mark, K.-W. Su, M. Seda, J. Hosek, and J.-S. Leu, "The minimization of public facilities with enhanced genetic algorithms using war elimination," *IEEE Access*, vol. 7, pp. 9395–9405, 2019.
[33] P. K. Jamwal, B. Abdikenov, and S. Hussain, "Evolutionary optimization using equitable fuzzy sorting genetic algorithm (EFSGA)," *IEEE Access*, vol. 7, pp. 8111–8126, 2019.
[34] *Space Engineering Spacecraft Mechanical Loads Analysis Handbook*, European Space Agency Standard, ECSS-E-HB-32-26A, Rev. ECSS-E-HB-32-26A, 2013.
[35] H. Ren and F. Chen, "Improvement of adaptive genetic algorithms and application in line simplification," (in Chinese), *Comput. Eng. Appl.*, vol. 48, no. 11, pp. 152–155, 2012.
[36] *Environmental Test Methods and Engineering Guidelines, Department of Defense Test Method Standard*, Department of Defense Test Method Standard, MIL-STD-810D, Rev. MIL-STD-810D, 1983.
[37] A. Aleti and L. Grunske, "Test data generation with a Kalman filter-based adaptive genetic algorithm," *J. Syst. Softw.*, vol. 103, pp. 343–352, May 2015.
[38] O. A. Abdul-Rahman, M. Munetomo, and K. Akama, "An adaptive parameter binary-real coded genetic algorithm for constraint optimization problems: Performance analysis and estimation of optimal control parameters," *Inf. Sci.*, vol. 233, pp. 54–86, Jun. 2013.
[39] M. Yu, H. Li, W. Jiang, H. Wang, and C. Jiang, "Fault diagnosis and rul prediction of nonlinear mechatronic system via adaptive genetic algorithm-particle filter," *IEEE Access*, vol. 7, pp. 11140–11151, 2019.

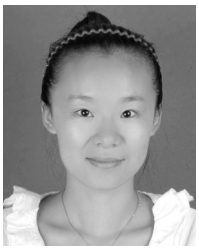

WENJUAN SUN received the M.S. degree in detection technology and automation device from the University of Science and Technology of China, Hefei, Anhui, China, in 2012, where she is currently pursuing the Ph.D. degree in mechanics.

She has been a Lecturer with Anhui Xinhua University, Hefei, since 2013. Her research interests include pyroshock response, optimization algorithms, and fatigue life prediction.

YINGQING HUANG received the M.S. and Ph.D. degrees in mechanics from the University of Science and Technology of China, Hefei, China, in 1994 and 1997, respectively, where he is currently an Associate Professor with the Department of Modern Mechanics. His research interests include high performance finite element method and meshless method.

HAIBO CHEN received the Ph.D. degree in mechanics from the University of Science and Technology of China, Hefei, China, in 1996.

From 1996 to 2000, he was a Lecturer with the University of Science and Technology of China; then he was an Associate Professor, from 2000 to 2005; he has been a Full Professor, since 2005. He was a Visiting Researcher with Cardiff University, in 1998. He was a Humboldt Research Follow with Karlsruhe University, from 1999 to 2001, and a Visiting Professor with Shinshu University, in 2007. His research interests include computational mechanics and engineering applications and vibration engineering. He is the editorial board member of Engineering Analysis with Boundary Elements and Current Mechanics and Advanced Materials. He is the member of International Association of Computational Mechanics.